Available online at www.sciencedirect.com
SCIENCE DIRECT®
Polymer 44 (2003) 4573–4588
polymer
www.elsevier.com/locate/polymer

Effect of hydrogen bonding on the rheology of polycarbonate/organoclay nanocomposites

Kyung Min Lee, Chang Dae Han*

Department of Polymer Engineering, The University of Akron, Akron, OH 44325-0301, USA

Received 7 February 2003; received in revised form 8 May 2003; accepted 14 May 2003

Abstract

The linear dynamic viscoelastic properties and non-linear transient rheology of polycarbonate (PC)/clay nanocomposites were investigated at temperatures ranging from 240 to 280 °C. For the study, nanocomposites of PC and natural montmorillonite (Cloisite Na^+) or chemically modified clay (Cloisite 30B) were prepared by melt blending in a twin-screw extruder. Cloisite 30B is a natural montmorillonite modified with methyl, tallow, bis-2-hydroxyethyl, quaternary ammonium chloride (MT2EtOH). In both PC/Cloisite Na^+ and PC/Cloisite 30B nanocomposites the concentration of clay was varied from 2.3 to 4.3 wt%. In situ Fourier transform infrared (FTIR) spectroscopy results show that at temperatures ranging from 30 to 280 °C the carbonyl groups in PC and the hydroxyl groups in MT2EtOH of Cloisite 30B in PC/Cloisite 30B nanocomposites formed hydrogen bonds, while no evidence of hydrogen bonding was observed in the PC/Cloisite Na^+ nanocomposites. There are no discernible sharp reflections in the X-ray diffraction (XRD) patterns of PC/Cloisite 30B nanocomposites, after Cloisite 30B having the d_{001} spacing of 1.85 nm was mixed with PC, whereas the d_{001} spacing changes little (1.17 nm) before and after the mixing of Cloisite Na^+ to PC. Transmission electron microcopy (TEM) images show that organoclay platelets are well dispersed in PC/Cloisite 30B nanocomposites, while the untreated clay platelets are poorly dispersed in PC/Cloisite Na^+ nanocomposites. The observed differences in XRD patterns and TEM images between the two nanocomposite systems are explained by in situ FTIR spectroscopy. The results of rheological measurements (linear dynamic viscoelasticity, non-linear transient shear flow, and steady-state shear flow) support the conclusions drawn from the results of XRD, TEM, and FTIR spectroscopy.

Keywords: Nanocomposites; Hydrogen bonding

1. Introduction

In recent years, clay-based nanocomposites have attracted much attention from both industry and academia. Clay-based nanocomposites are produced by combining a thermoplastic polymer and about 1 nm-thick silicate layers of clay minerals. One of the advantages of nanocomposites lies in that the concentration of nanometer-size platelets required is much lower (say less than 7 wt%) than that (say 40–50 wt%) required for the conventional highly filled thermoplastic composites. Thus, the weight-to-volume ratio of nanocomposites is much lower than that of the conventional thermoplastic composites, which then offers a distinct advantage in that less energy would be required when such nanocomposites are processed for automotive or aerospace applications, for example. However, the key to a successful development of clay-based nanocomposites is to match chemical affinity between the polymer matrix and the silicate layers of clay. This means that as in the preparation of polymer blends having improved mechanical properties, polymer matrix and silicate layers of clay must be compatible. Therefore, it is essential to chemically modify a natural clay, such that it can become compatible with a chosen thermoplastic polymer and/or to chemically modify a thermoplastic polymer that can be compatible with a chemically modified clay.

Among the thermoplastic polymers, nylon 6 is one of the few that has met with commercial success and thus many investigators reported on clay-based nanocomposites with nylon 6 [1–6]. Other polymers, such as polystyrene [7,8], polypropylene [9–13], poly(ε-caprolactone) [14], and poly(ethylene oxide) [15,16], also have been employed to develop clay-based nanocomposites. There are too many

* Corresponding author. Tel.: +1-330-972-6468; fax: +1-330-972-5720.
E-mail address: cdhan@uakron.edu (C.D. Han).

0032-3861/03/$ - see front matter © 2003 Elsevier Science Ltd. All rights reserved.
doi:10.1016/S0032-3861(03)00444-0

papers to cite them all here, and the readers are referred to a recent paper by Sur et al. [17] who cited 206 references.

The processing of nanocomposites requires information on their rheological properties. During the past decade, a large number of papers have been published, which dealt with the rheology of layered silicate-based nanocomposites. Today, it is well established that when a thermoplastic polymer is melt blended with layered silicates, it either intercalates or exfoliates the layered silicates. In general, intercalation is observed when a polymer matrix and layered silicates do not have attractive interactions, while exfoliation is observed when a polymer matrix and layered silicates have strong attractive interactions. Thermodynamic aspects of intercalation and exfoliation in the preparation of nanocomposites have been investigated [18–23]. From the point of view of obtaining markedly improved physical/mechanical properties of nanocomposites, exfoliation is preferred to intercalation. In view of the fact that strong attractive interactions between a polymer and layered silicates are required to achieve exfoliation (or markedly improved dispersion of layered silicates) in a nanocomposite, some serious attempts have been made to induce attractive interactions when a polymer and layered silicates are melt blended. For this reason, much effort has been spent on chemical modifications of layered silicates. Below, for simplicity, we shall refer to chemically modified layered silicates as 'organoclays'. More often than not, thermoplastic polymers that are to be mixed with organoclays have no functional group. Under such circumstances, one must introduce a functional group(s) into a thermoplastic polymer in order to induce attractive interactions with organoclays during melt blending (or solution blending). However, there is more than one approach to induce attractive interactions.

One approach to induce attractive interactions between a polymer and layered silicates is to employ a third component, commonly referred to as compatibilizing agent, which then can help improve compatibility between the polymer chosen and the organoclay. Indeed such an approach has been used to investigate the rheology of nanocomposites. Specifically, some investigators [24] employed polystyrene (PS) grafted with maleic anhydride (MA), PS-*g*-MA, as compatibilizing agent to prepare nanocomposites consisting of PS and organoclays, while others [25,26] employed polypropylene (PP) grafted with MA, PP-*g*-MA, as compatibilizing agent to prepare nanocomposites consisting of PP and organoclays. However, these studies did not elucidate a mechanism(s) that has led to the unusual rheological behavior observed.

Another approach to induce attractive interactions between a thermoplastic polymer and organoclays in the preparation of nanocomposites is to perform in situ polymerization in the presence of organoclays. This interesting concept was used by Giannelis and Krishnamoorti [27–29] and also by other investigators [30,31]. Specifically, Giannelis and Krishnamoorti induced ionic interaction between poly(ε-caprolactone) and negatively charged layered silicates by first mixing layered silicates in the monomer of ε-caprolactone and then polymerizing ε-caprolactone in the presence of the modified layered silicate. This approach has yielded end-tethered poly(ε-caprolactone) layered silicate nanocomposites, in which the majority of the polymer chains are tethered to the surface of the layered silicates. The ionic interaction has produced unusual rheological behavior [27–29]. Hoffmann and co-workers [30] also reported on unusual rheological behavior of end-tethered layered silicate nanocomposites, which were obtained by polycondensation of ω-aminododeanic acid in an autoclave in the presence of the swollen layered silicates and then by mixing with polyamide 12. They attributed the unusual rheological behavior observed to the formation of a network involving assembly of individual platelets being composed of silicate layers.

In the present study, we have investigated the linear dynamic viscoelastic properties, transient shear flow, intermittent shear flow after rest for a predetermined period upon cessation of steady shear flow, and steady-state shear flow of polycarbonate (PC)/organoclay nanocomposites and PC/natural clay nanocomposites. The organoclay employed has hydroxyl groups residing at the surface of the silicate layers of clay aggregates. Since the organoclay chosen had hydroxyl groups, we chose PC to prepare nanocomposites with the expectation that, the carbonyl group in PC would form hydrogen bonds, during melt blending, with the hydroxyl group present on the surface of the organoclay chosen. Thus, in our study we did not have to chemically modify PC or employ a compatibilizing agent in order to induce attractive interactions between PC and the organoclay. We have found significant differences in rheological responses between the two nanocomposite systems, one with organoclay and the other with natural clay. The observed differences in rheological responses between the two nanocomposite systems are explained using the experimental results of in situ Fourier transform infrared spectroscopy, showing evidence that hydrogen bonding took place between the carbonyl groups in PC and the hydroxyl groups in the organoclay. Using transmission electron microscopy we have found that the dispersion of layered silicates of organoclay aggregates is significantly improved compared to that of layered silicates of natural clay aggregates in PC. This finding is supported by the results of X-ray diffraction. In this paper we report the highlights of our findings.

2. Experimental

2.1. Materials and preparation of nanocomposites

In this study we employed two types of clay received from Southern Clay Products: (i) natural montmorillonite (Cloisite Na^+) and (ii) an organoclay (Cloisite 30B) which is a natural montmorillonite modified with a surfactant

(MT2EtOH): methyl, tallow, bis-2-hydroxyethyl, quaternary ammonium chloride with the chemical structure [32]

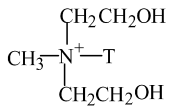

MT2EtOH

where N^+ denotes quaternary ammonium chloride and T denotes tallow consisting of ~65% C18, ~30% C16, and ~5% C14. The amount of surfactant (MT2EtOH) in Cloisite 30B is 32 wt%, and 100% of the Na^+ ions have been exchanged. Notice that the surfactant MT2EtOH has unsaturated aliphatic chains and two hydroxyl groups.

Polycarbonate (Iupilon E2000, Mitsubishi Gas Company, Japan) in the form of flake was dried for 12 h prior to melt blending and the clays were used as received. Using a co-rotating twin-screw extruder we melt blended each of the above two clays with PC to prepare nanocomposites, for which the temperature was controlled at 260 °C and the extrudate was pelletized. The pelletized nanocomposites were dried and then injection molded at 280 °C by keeping the mold temperature at 90 °C. The visual appearance of the injection-molded specimens of 97.7/2.3 PC/Cloisite 30B nanocomposite was light brown, and the visual appearance of the injection-molded specimens of 95.7/4.3 PC/Cloisite 30B nanocomposite was dark brown.

The concentrations of Cloisite Na^+ or Cloisite 30B in the respective nanocomposites were 2.3 and 4.3 wt%. Since the amount of surfactant (MT2EtOH) in Cloisite 30B is about 32 wt%, the net amount of clay is 1.56 wt% in the nanocomposite containing 2.3 wt% organoclay and 2.92 wt% in the nanocomposite containing 4.3 wt% organoclay.

2.2. X-ray diffraction (XRD)

Using a Rigaku X-ray generator operated at 50 kV and 150 mA X-ray diffraction patterns were obtained to determine the mean interlayer spacing (gallery distances) of the (001) plane (d_{001}) for natural montmorillonite (Cloisite Na^+), organoclay (Cloisite 30B), PC/Cloisite Na^+ nanocomposite, and PC/Cloisite 30B nanocomposite. The range of 2θ scanning of X-ray intensity employed was 1.5–10°. Before XRD experiment, specimens were annealed in a vacuum oven at 200 °C for 1 week to remove moisture completely.

2.3. Transmission electron microscopy (TEM)

TEM images of nanocomposite specimens without staining were taken at room temperature. The ultrathin sectioning (50–70 nm) was performed by ultramicrotomy at room temperature using a Reichert Ultracut E low-temperature sectioning system. A transmission electron microscope (JEM1200EX 11, JEOL) operated at 120 kV was used to obtain images of the nanocomposite specimens. Before TEM experiment, specimens were annealed in a vacuum oven at 200 °C for 1 week to remove moisture completely.

2.4. Fourier transform infrared (FTIR) spectroscopy

Using a Fourier Transform Infra-Red Spectrometer (16 PC FTIR, Perkin–Elmer), in situ FTIR spectra were obtained at various temperatures ranging from 30 to 280 °C for neat PC, 95.7/4.3 PC/Cloisite Na^+ nanocomposite, and 95.7/4.3 PC/Cloisite 30B nanocomposite. Spectral resolution was maintained at 4 cm^{-1}. The temperature was measured at the sample surface and controlled within ±1.0 °C using a proportional-integral-derivative controller. Specimens were maintained at a preset temperature for 5 min prior to data acquisition. Dry argon gas was used to purge the sample compartment in order to reduce the interference of water and carbon dioxide in the spectrum. For FTIR spectroscopic experiment, thin films of the thickness of about 0.1 mm were prepared by compression molding at 240 °C. Before FTIR spectroscopic experiments, specimens were annealed in a vacuum oven at 200 °C for 1 week to remove moisture completely.

2.5. Thermal characterization

Thermal transition temperatures of PC, 95.7/4.3 PC/Cloisite Na^+ nanocomposite, and 95.7/4.3 PC/Cloisite 30B nanocomposite were determined using differential scanning calorimetry (DSC) (Model DSC 2920, TA Instrument) under a nitrogen atmosphere, at a heating rate of 20 °C min^{-1}. Also, thermogravimetric analysis (Model TGA 2050, TA Instrument) was conducted to investigate the extent of thermal degradation of PC, Cloisite 30B, and PC/Cloisite 30B nanocomposite at elevated temperatures under a nitrogen atmosphere at a heating rate of 10 °C min^{-1}. The thermal history of the specimens employed for TGA was the same as that employed for XDR, TEM, FTIR, and rheological measurements.

2.6. Rheological measurements

An Advanced Rheometric Expansion System (ARES, Rheometric Scientific) with a parallel-plate fixture (25-mm diameter) was used to conduct dynamic frequency sweep experiments of the nanocomposites, measuring the storage and loss moduli (G' and G'') as functions of angular frequency (ω) (ranging from 0.01 to 100 rad s^{-1}) at 240, 260, and 280 °C. In conducting oscillatory shear measurements, the following protocols were employed. A specimen was first placed in the preheated parallel-plate fixture, and then the gap setting was adjusted to about 2 mm by squeezing. After the temperature of the specimen was equilibrated, we monitored normal force signal to make certain that it reached the baseline (i.e. zero normal force). This was because squeezing of a specimen generated normal

stress in the specimen. Since the nanocomposite samples employed in the present study were virtually inelastic, we found that the time required for the residual stress, which was accumulated during squeezing, to relax took a relatively short time (less than 10 min), compared to our previous experiences with thermotropic liquid crystalline polymers. Only after we ascertained that the normal force signal reached the baseline, did we commence oscillatory shear experiments. Using such a protocol, we were able to obtain reproducible data. In the oscillatory shear measurements, a fixed strain of 0.04 was used to ensure that measurements were taken well within the linear viscoelastic range of the materials investigated. The frequency sweep experiment at a preset temperature lasted for about 45 min, while the temperature control was accurate to within ± 1 °C. We also conducted experiments of transient shear flow, intermittent shear flow after rest for a predetermined period upon cessation of shear flow, and steady-state shear flow for different shear rates at 240, 260, and 280 °C using the cone-and-plate fixture (25-mm diameter). The experimental protocols employed for the transient and steady-state shear experiments were virtually the same as that for the oscillatory shear experiments described above, except for that the gap setting of the cone-and-plate fixture was 50 μm. Only after we ascertained that the normal force signal reached the baseline, did we commence transient shear flow (until steady state was reached). Using such a protocol, we were able to obtain reproducible data. All measurements were conducted under a nitrogen atmosphere to avoid oxidative degradation of the specimens.

For rheological experiment, injection-molded specimens were cut into small pieces about 2 cm diameter disks. Before rheological measurements, specimens were annealed in a vacuum oven at 200 °C for 1 week to completely remove moisture.

3. Results and discussion

3.1. X-ray diffraction (XRD) patterns of PC/Cloisite Na^+ and PC/Cloisite 30B nanocomposites

Fig. 1 shows XRD patterns of a natural montmorillonite Cloisite Na^+, an organoclay Cloisite 30B, 95.7/4.3 PC/Na^+ nanocomposite, and 95.7/4.3 PC/Cloisite 30B nanocomposite. The XRD patterns in Fig. 1 show that Cloisite Na^+ has a d_{001} spacing of 1.17 nm while Cloisite 30B has a d_{001} spacing of 1.85 nm. The XRD patterns shown in Fig. 1 indicate that the d_{001} spacing of the 95.7/4.3 PC/Cloisite Na^+ nanocomposite is ca. 1.31 nm, which is slightly higher than that (1.17 nm) of Cloisite Na^+. On the other hand, in Fig. 1 we observe *no* sharp reflections in the XRD pattern of 95.7/4.3 PC/Cloisite 30B nanocomposite. The lack of discernible intensity peak in Fig. 1 for the 95.7/4.3 PC/Cloisite 30B nanocomposite indicates that a significant degree of dispersion of the organoclay aggregates has occurred by the PC having carbonyl groups. As for the mechanism of dispersion of organoclay (Cloisite 30B) aggregates by the PC, the driving force is believed to have originated from the hydrogen bonding, as will be shown below by in situ FTIR spectra, between the carbonyl groups in PC and the hydroxyl groups in MT2EtOH residing at the surface of silicate layers of Cloisite 30B.

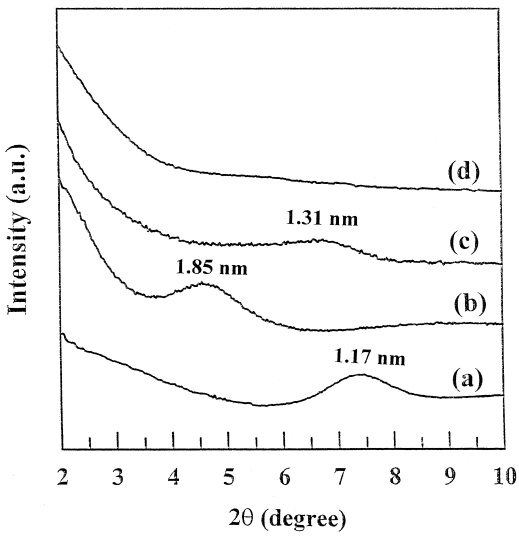

Fig. 1. X-ray diffraction patterns for: (a) Cloisite Na^+, (b) Cloisite 30B, (c) 95.7/4.3 PC/Cloisite Na^+ nanocomposite, and (d) 95.7/4.3 PC/Cloisite 30B nanocomposite.

3.2. The state of dispersion of layered silicate aggregates in PC/Cloisite Na^+ and PC/Cloisite 30B nanocomposites

Fig. 2 shows TEM images of (a) 95.7/4.3 PC/Cloisite 30B nanocomposite and (b) 95.7/4.3 PC/Cloisite Na^+ nanocomposite, where the dark areas represent the clay and the gray/white areas represent the PC matrix. It is clearly seen in Fig. 2 that PC in the 95.7/4.3 PC/Cloisite 30B nanocomposite has dispersed the organoclay aggregates fairly well, whereas PC in the 95.7/4.3 PC/Cloisite Na^+ nanocomposite has not (i.e. large aggregates of natural clay are bundled together), indicating that the carbonyl groups in PC must have played the major role in dispersing the organoclay aggregates, leading to a significant degree of dispersion of the silicate layers of organoclay (Cloisite 30B) aggregates. The better dispersed the organoclay aggregates are, the larger will be the surface areas of the silicate layers of organoclay that become available for specific interactions (i.e. hydrogen bonding), as will be shown below by FTIR spectra, with the carbonyl groups in PC, which will in turn help increase the degree of dispersion (or exfoliation) of organoclay aggregates.

3.3. FTIR spectroscopy of PC/Cloisite 30B and PC/Cloisite Na^+ nanocomposites

In an effort to search for evidence that may support or

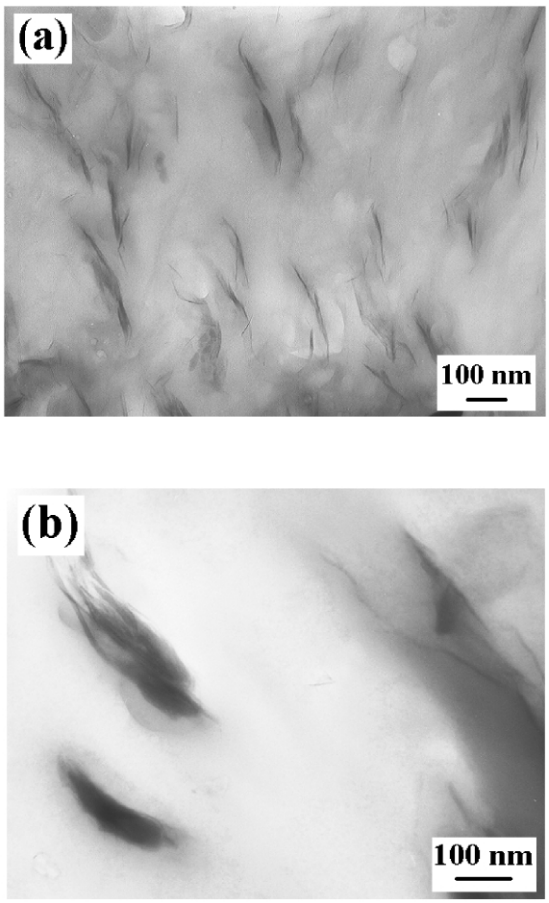

Fig. 2. TEM images of (a) 95.7/4.3 PC/Cloisite 30B nanocomposite and (b) 95.7/4.3 PC/Cloisite Na^+ nanocomposite, where the dark areas represent the clay and the gray/white areas represent the PC matrix.

reject the postulations made above, in this study we have conducted in situ FTIR spectroscopy experiment at various temperatures ranging from 30 to 280 °C for (i) neat PC, (ii) 95.7/4.3 PC/Cloisite Na^+ nanocomposite, and (iii) 95.7/4.3 PC/Cloisite 30B nanocomposite, and the results are shown in Fig. 3. In Fig. 3a, the absorption band for PC appears at ca. 1775 cm^{-1} representing the free carbonyl stretching vibration peak [33,34]. Similar observation can be made in Fig. 3b for 95.7/4.3 PC/Cloisite Na^+ nanocomposite, indicating that *few* molecular interactions take place between PC and natural clay, Cloisite Na^+. However, in Fig. 3c we observe two stretching peaks, one peak at about 1790 cm^{-1} that is attributable to the free carbonyl stretching peak and another peak at about 1750 cm^{-1} that is attributable to the hydrogen-bonded carbonyl stretching peak in the 95.7/4.3 PC/Cloisite 30B nanocomposite. The hydrogen-bonded carbonyl stretching peak appearing at about 1750 cm^{-1} is believed to be due to the specific interactions between the carbonyl groups in PC and the hydroxyl groups in MT2EtOH of organoclay in the 95.7/4.3 PC/Cloisite 30B nanocomposite.

We attempted to determine the percentage of hydrogen-bonding sites on the organoclay (Cloisite 30B) surface by

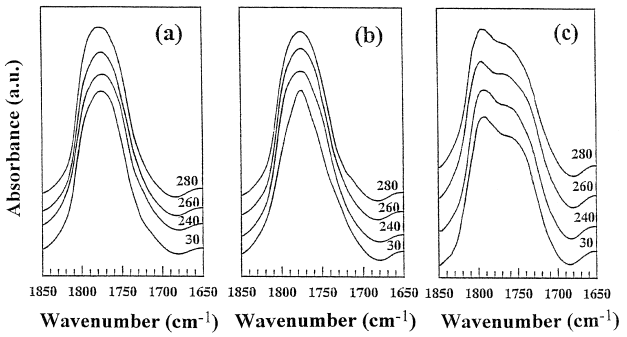

Fig. 3. FTIR spectra at various temperatures for: (a) PC, (b) 95.7/4.3 PC/Cloisite Na^+ nanocomposite, and (c) 95.7/4.3 PC/Cloisite 30B nanocomposite.

deconvoluting the overlapping peaks in the FTIR spectra shown in Fig. 3c. However, we found this to be a very difficult task, if not impossible, since the amount of surfactant MT2EtOH in each nanocomposite was very small: ca. 0.75 wt% in the 97.7/2.3 PC/Cloisite 30B nanocomposite and ca. 1.38 wt% in the 95.7/4.3 PC/Cloisite 30B nanocomposite. What made the situation worse was that an accurate determination, via ^1H nuclear magnetic resonance (NMR) spectroscopy, of the amount of the hydroxyl groups in the surfactant MT2EtOH was extremely difficult owing to the very complex nature of its chemical structure. That is, from the ^1H NMR spectra it was difficult to identify the protons associated with the hydroxyl groups, since there were so many protons that were associated with the unsaturated double bonds of the tallow. We have concluded that further pursuit of this subject is beyond the primary objective of this study.

Earlier, the presence of hydrogen bonds between the carbonyl groups in poly(4-vinyl phenol) (PVPh) and the hydroxyl groups in poly(vinyl acetate) (PVAc) in a PVPh/PVAc blend has been demonstrated, as depicted below [35]:

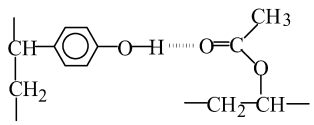

According to Painter and Coleman [33,34], the stretching band representing free carbonyl groups in PVAc appears at 1739 cm^{-1} and the stretching band representing the PVAc acetoxy carbonyl groups hydrogen bonded to the phenolic hydroxyl group of PVPh appears at 1714 cm^{-1}. They noted that the specific interactions, via hydrogen bonding, between the carbonyl groups in PVAc and the hydroxyl groups in PVPh have made the PVAc/PVPh blends miscible.

Notice in Fig. 3c that the hydrogen-bonded band (1750 cm^{-1}) appears as a shoulder and is not well resolved. This is understandable, because the amount of hydroxyl groups in the 95.7/4.3 PC/Cloisite 30B nanocomposite is very small in that the amount of organoclay Cloisite 30B in the nanocomposite is only 4.3 wt% and further Cloisite 30B

contains 32 wt% MT2EtOH, which in turn has small amounts of hydroxyl groups (see the chemical structure of MT2EtOH given in Section 2). It is of great interest to observe in Fig. 3c that the area under the absorption band at about 1750 cm^{-1} for the 95.7/4.3 PC/Cloisite 30B nanocomposite remains more or less constant over the entire range of temperatures investigated from 30 to 280 °C. The above observation seems to indicate that the strength of hydrogen bonds between the carbonyl groups in PC and the hydroxyl group in MT2EtOH of Cloisite 30B persists up to 280 °C. This observation stands in contrast with the observation made in our recent study [36], in which we reported that the strength of hydrogen bonds between the hydroxyl groups in a polystyrene-*block*-hydroxylated polyisoprene copolymer and the hydroxyl group in MT2EtOH of Cloisite 30B decreased with increasing temperature. Thus, we can conclude from Fig. 3 that the specific interactions, via hydrogen bonding, exist between the carbonyl group in PC and the hydroxyl group in MT2EtOH of Cloisite 30B in the 95.7/4.3 PC/Cloisite 30B nanocomposite, whereas no specific interactions exist between PC and natural clay in the 95.7/4.3 PC/Cloisite Na^+ nanocomposite.

3.4. Glass transition temperatures of 95.7/4.3 PC/Cloisite Na^+ and 95.7/4.3 PC/Cloisite 30B nanocomposites

Fig. 4 shows DSC traces for (1) PC, (2) 95.7/4.3 PC/Cloisite Na^+ nanocomposite, and (3) 95.7/4.3 PC/Cloisite 30B nanocomposite, which were obtained in the second heating at a rate of 20 °C min^{-1}. We also conducted DSC experiments at two additional heating rates, 5 and 10 °C min^{-1}, for both 95.7/4.3 PC/Cloisite 30B and 97.7/2.3 PC/Cloisite 30B nanocomposites. We have found, although DSC traces are not presented here, that the T_g of PC/Cloisite 30B nanocomposites is lowered by ca. 5 °C as the heating rate is decreased from 20 to 10 °C min^{-1}, and by ca. 8 °C as the heating rate is decreased from 20 to 5 °C min^{-1}. Further, we found that the T_g of the 95.7/4.3 PC/Cloisite 30B nanocomposite is about 2–3 °C higher than that of the 97.7/2.3 PC/Cloisite 30B nanocomposite. We wish to point out, however, that the effect of organoclay concentration and the heating rate dependence of T_g have little to do with the main theme (the effect of hydrogen bonding on the rheology of PC/organoclay nanocomposites) of our study reported herein. This is because our rheological measurements were taken at 240–280 °C, which are far above the T_g (155–167 °C depending on the heating rate) of the nanocomposites. It is very interesting to observe in Fig. 4 that the glass transition temperature (T_g) of 95.7/4.3 PC/Cloisite Na^+ nanocomposite is lower by 7 °C, while the T_g of 95.7/4.3 PC/Cloisite 30B nanocomposite is higher by 10 °C, as compared to the T_g of neat PC. This observation is consistent with the observations made above from the XRD patterns (Fig. 1), TEM images (Fig. 2), and FTIR spectra (Fig. 3) that the carbonyl groups in PC and the hydroxyl groups in the surfactant (MT2EtOH) have induced attractive interactions, resulting with an enhanced compatibility between the PC matrix and the organoclay, Cloisite 30B. Notice in Fig. 4 that in the *absence* of attractive interaction between the PC matrix and the natural montmorillonite (Cloisite Na^+) having *no* functional group, the T_g of the 95.7/4.3 PC/Cloisite Na^+ nanocomposite is decreased from 157 °C for neat PC to 150 °C.

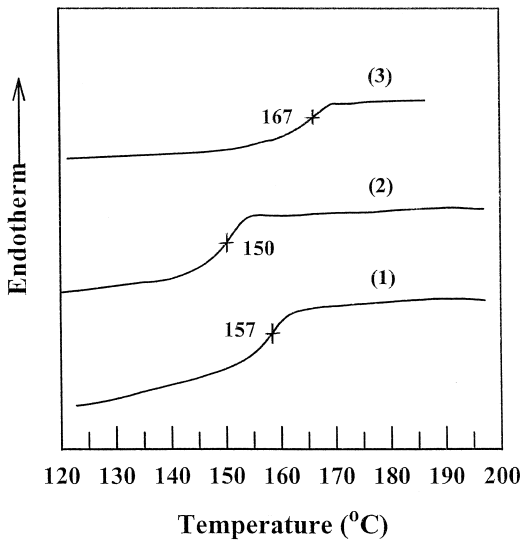

Fig. 4. DSC traces for (1) PC, (2) 95.7/4.3 PC/Cloisite Na^+ nanocomposite, and (3) 95.7/4.3 PC/Cloisite 30B nanocomposite in the second heating at a rate of 20 °C min^{-1}.

3.5. Thermal degradation characteristics of polycarbonate, Cloisite 30B, and PC/Cloisite 30B nanocomposite

We investigated, via TGA, the extent to which thermal degradation might have affected the linear viscoelastic properties summarized above. Fig. 5 shows TGA traces for (a) PC, (b) Cloisite 30B, and (c) 95.7/4.3 PC/Cloisite 30B nanocomposite at temperatures up to about 400 °C, which were obtained at a heating rate of 10 °C min^{-1} under a nitrogen atmosphere. The following observations are worth noting in Fig. 5. At 280 °C, PC has a weight loss of 0.4%, Cloisite 30B has a weight loss of 7.8%, and 95.7/4.3 PC/Cloisite 30B nanocomposite has a weight loss of 0.6%. Since Cloisite 30B has 32 wt% of surfactant (MT2EtOH), the net weight loss of MT2EtOH in the Cloisite 30B at 280 °C is 24.4%. On the other hand, the net loss of MT2EtOH in the 95.7/4.3 PC/Cloisite 30B nanocomposite at 280 °C is 14.6 wt%, because the loss of 0.6 wt% in the nanocomposite includes the loss of 0.4 wt% of PC and thus the net loss of MT2EtOH alone is 0.2 wt%. Note that the amount of MT2EtOH in the 95.7/4.3 PC/Cloisite 30B nanocomposite is 1.37 wt%, because Cloisite 30B contains 32 wt% of MT2EtOH. What is most interesting from the above observations is that the net loss (14.6 wt%) of MT2EtOH in the 95.7/4.3 PC/Cloisite 30B nanocomposite

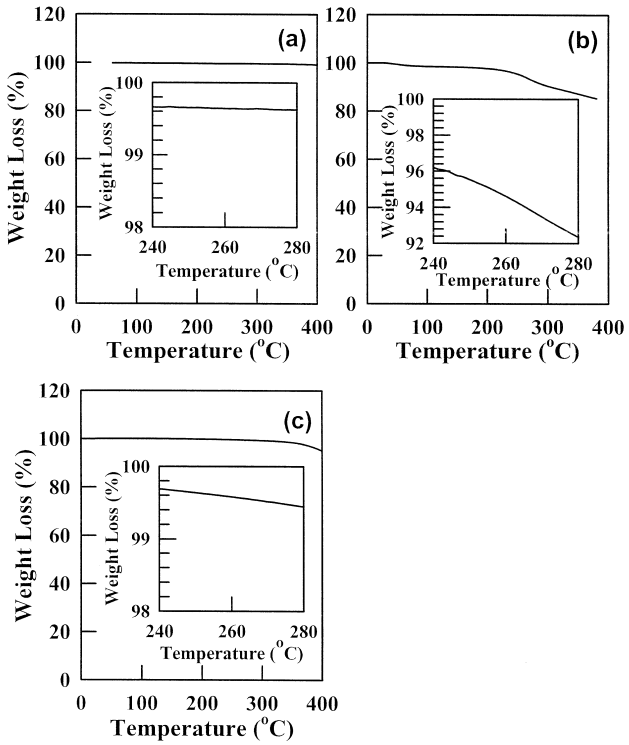

Fig. 5. TGA traces for (a) PC, (b) Cloisite 30B, and (c) 95.7/4.3 PC/Cloisite 30B nanocomposite, which were obtained at a heating rate of 10 °C min^{-1} under a nitrogen atmosphere.

is about one half the net loss (24.4 wt%) of MT2EtOH in the Cloisite 30B. The lesser degree of thermal degradation of MT2EtOH observed in the 95.7/4.3 PC/Cloisite 30B nanocomposite, as compared to that in Cloisite 30B alone, may be explained by the argument in that the PC penetrated (or diffused) into the gallery of Cloisite 30B platelets might have retarded thermal degradation and diffusion of MT2EtOH, relative to the situation where MT2EtOH is present at the surface of layered silicate aggregates without any polymers penetrated (or diffused) into the gallery.

Further evidence that the extent of thermal degradation of MT2EtOH in the 95.7/4.3 PC/Cloisite 30B nanocomposite at temperatures up to 280 °C is insignificant is manifested by the FTIR spectrum shown in Fig. 3c, in which we observe that the area under the shoulder at the absorption band in the vicinity of 1750 cm^{-1}, which represents the hydrogen-bonded carbonyl stretching peak, remains virtually constant over the temperatures ranging from 30 to 280 °C. In other words, if the extent of thermal degradation of MT2EtOH had been significant, we should not have observed the same area under the shoulder at the absorption band at 1750 cm^{-1}.

Very recently, Xie et al. [37,38] investigated thermal degradation of several organically modified (alkyl quaternary ammonium) layered silicates (OLS) using TGA, and TGA combined with FTIR spectroscopy and mass spectrometry (TG-FTIR-MA). They [37] reported that the onset temperature of decomposition of the OLSs was approximately 155 °C, and the weight loss between 120 and 450 °C of the OLSs having trimethylalkyl in the surfactant was in the range of 17–23%, which is in agreement with our result (24.4%) summarized above for Cloisite 30B. However, Xie et al. did not report on the extent of any thermal degradation of surfactant in the polymer nanocomposites.

3.6. Linear dynamic viscoelastic properties of PC/Cloisite Na^+ and PC/Cloisite 30B nanocomposites

To facilitate our discussion later in this paper, (a) log G' versus log ω plots and (b) log G'' versus log ω plots for PC at 240, 260, and 280 °C are shown in Fig. 6, showing that values of G' and G'' decrease with increasing temperature. It is seen in Fig. 6 that in the terminal region, the slope of log G' versus log ω plots is very close to 2 and the slope of log G'' versus log ω plots is very close to 1, such linear dynamic viscoelastic behavior being expected for homopolymers. The steady decrease in G' as the temperature is increased from 240 to 280 °C seems to indicate that any thermal degradation of PC within that temperature range has an insignificant effect on the values of G' measured. We conducted additional dynamic frequency sweep experiments for the PC at 200 °C, although the results of which are not presented here, in order to find out whether or not it exhibited a plateau region. We have found no evidence of a plateau region in the log G' versus log ω plots over the angular frequencies ranging from 10^{-2} to 10^{2} rad s^{-1} and thus we have concluded that the molecular weight of the PC employed in this study is too low to have a plateau modulus (i.e. the PC must be regarded as consisting of Rouse chains).

Fig. 7 shows the effect of temperature on log G' versus log ω plots for (a) 97.7/2.3 PC/Cloisite Na^+ nanocomposite and (b) 95.7/4.3 PC/Cloisite Na^+ nanocomposite, where 97.7/2.3 and 95.7/4.3, respectively, refer to the wt% of PC and Cloisite Na^+ in the nanocomposite. It is seen in Fig. 7 that the slope of the log G' versus log ω plot in the terminal region is less than 2, and values of G' decrease as the temperature is increased. An increase in the Cloisite Na^+ concentration from 2.3 to 4.3 wt% has had little effect on the values of G' in the low frequency region (for $\omega < 1$ rad s^{-1}) but has decreased values of G' in the higher frequency

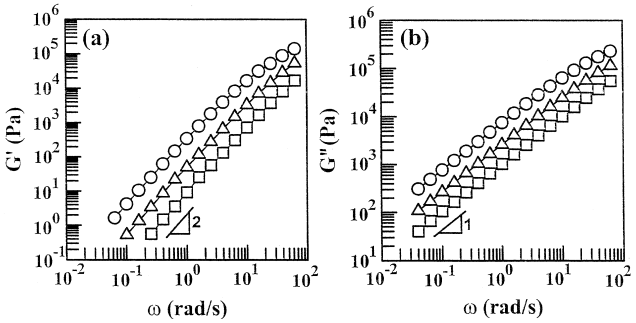

Fig. 6. Plots of (a) log G' versus log ω and (b) log G'' versus log ω for PC at various temperatures: (○) 240 °C; (△) 260 °C; (□) 280 °C.

region (for $\omega > 10$ rad s^{-1}). Comparison of Fig. 7 with Fig. 6 reveals that values of G' for PC/Cloisite Na$^+$ nanocomposites are larger than those for neat PC in the low frequency region (for $\omega < 1$ rad s^{-1}), while an opposite trend is observed in the higher frequency region (for $\omega > 10$ rad s^{-1}).

Fig. 8 shows the effect of temperature on log G' versus log ω plots for (a) 97.7/2.3 PC/Cloisite 30B nanocomposite and (b) 95.7/4.3 PC/Cloisite 30B nanocomposite. The following observations are worth noting in Fig. 8. For the 97.7/2.3 PC/Cloisite 30B nanocomposite values of G' in the low frequency region (for $\omega <$ ca. 0.4 rad s^{-1}) increase with increasing temperature, while values of G' in the higher frequency region (for $\omega >$ ca. 0.4 rad s^{-1}) decrease with increasing temperature. The same trend is also observed for the 95.7/4.3 PC/Cloisite 30B nanocomposite. Interestingly, values of G' in the low frequency region (for $\omega <$ ca. 0.4 rad s^{-1}) are increased by about 1 order of magnitude as the concentration of Cloisite 30B is increased from 2.3 to 4.3 wt%. Such an observation is not made when natural clay (Cloisite Na$^+$) was added to PC (compare Fig. 8 with Fig. 7). Notice further in Fig. 8 that the slope of log G' versus log ω plots for PC/Cloisite 30B nanocomposites is decreased drastically, exhibiting solid-like behavior, as the temperature is increased from 240 to 280 °C.

The increase in G' at low values of ω with increasing temperature from 240 to 280 °C, observed in Fig. 8, for the PC/Cloisite 30B nanocomposites is attributable to the formation of hydrogen bonds between the carbonyl groups in PC and the hydroxyl groups in MT2EtOH. The readers are reminded that in Fig. 3c we have shown evidence of the formation of hydrogen bonds in the 95.7/4.3 PC/Cloisite 30B nanocomposite. The observed increase of G' in Fig. 8 cannot be ascribed to the formation of some products from PC and the gases decomposed from MT2EtOH, because at large values of ω, G' decreases with increasing temperature from 240 to 280 °C.

Fig. 9 shows the effect of the concentration of natural clay (Cloisite Na$^+$) on the linear viscoelastic dynamic moduli of PC/Cloisite Na$^+$ nanocomposites at 280 °C as functions of ω. Notice in Fig. 9a that an increase in the concentration of Cloisite Na$^+$ from 2.3 to 4.3 wt% has little

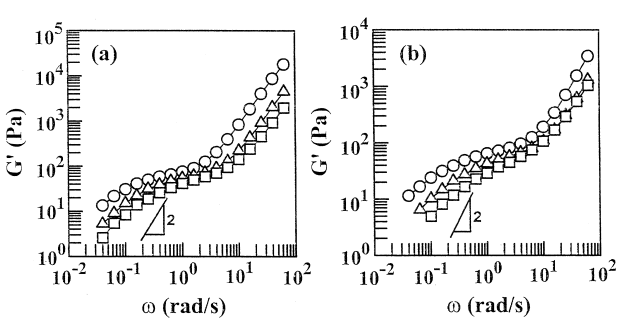

Fig. 7. Plots of log G' versus log ω for (a) 97.7/2.3 PC/Cloisite Na$^+$ nanocomposite and (b) 95.7/4.3 PC/Cloisite Na$^+$ nanocomposite at various temperatures: (○) 240 °C; (△) 260 °C; (□) 280 °C.

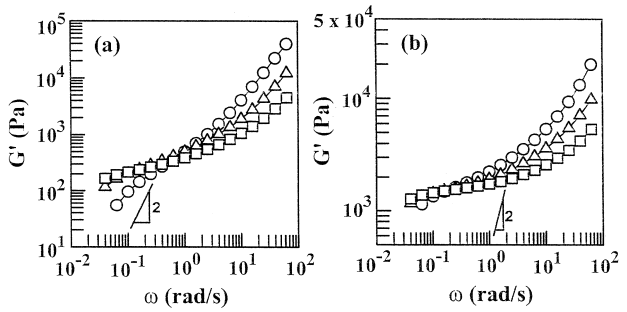

Fig. 8. Plots of log G' versus log ω for (a) 97.7/2.3 PC/Cloisite 30B nanocomposite and (b) 95.7/4.3 PC/Cloisite 30B nanocomposite at various temperatures: (○) 240 °C; (△) 260 °C; (□) 280 °C.

effect on the G' of PC/Cloisite Na$^+$ nanocomposite over the entire range of ω investigated. For comparison, also given in Fig. 9 are log G' versus log ω, and log G'' versus log ω plots for neat PC at 280 °C. It is seen in Fig. 9a that log G' versus log ω plot for the PC/Cloisite Na$^+$ nanocomposites cross that for neat PC at about $\omega = 3$ rad s^{-1}, showing that values of G' for the PC/Cloisite Na$^+$ nanocomposites are greater than those of neat PC at $\omega <$ ca. 3 rad s^{-1} while an opposite trend is observed at $\omega >$ ca. 3 rad s^{-1}. On the other hand, in Fig. 9b we observe that values of G'' for the PC/Cloisite Na$^+$ nanocomposites are less than those of neat PC over the entire range of ω investigated, and that the slope of log G'' versus log ω plot in the terminal region is slightly less than 1.

Fig. 10 shows the effect of the concentration of organoclay (Cloisite 30B) on the linear viscoelastic dynamic moduli of PC/Cloisite 30B nanocomposites at 280 °C as functions of ω. For comparison, also given in Fig. 10 are log G' versus log ω, and log G'' versus logω plots for neat PC at 280 °C. In Fig. 10a, we observe a very large effect of the concentration of Cloisite 30B on the G' of PC/Cloisite 30B nanocomposites; namely an increase of Cloisite 30B from 2.3 to 4.3 wt% has increased the values of G' of PC/Cloisite 30B nanocomposite in the low frequency region (for $\omega <$ ca. 0.1 rad s^{-1}) by about 1 order of magnitude. Notice that both 97.7/2.3 and 95.7/4.3 PC/Cloisite 30B nanocomposites exhibit solid-like behavior, in large contrast to the 97.7/2.3 and 95.7/4.3 PC/Cloisite Na$^+$

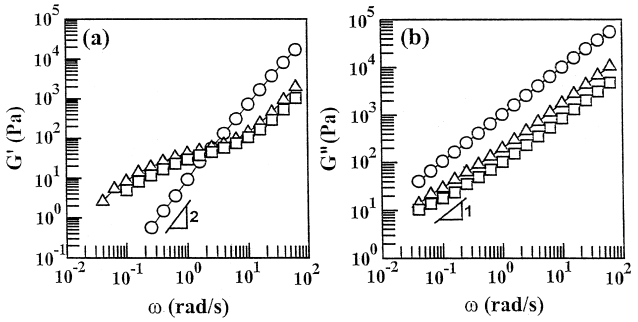

Fig. 9. Plots of (a) log G' versus log ω and (b) log G'' versus log ω at 280 °C for: (○) neat PC, (△) 97.7/2.3 PC/Cloisite Na$^+$ nanocomposite, and (□) 95.7/4.3 PC/Cloisite Na$^+$ nanocomposite.

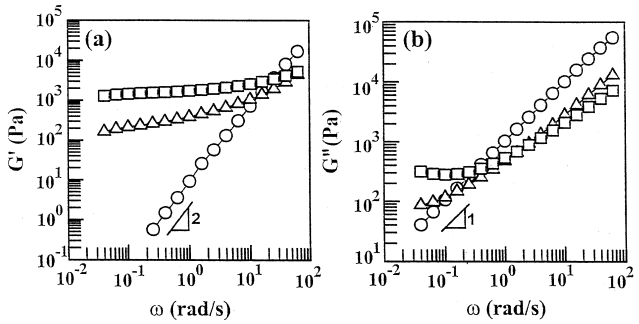

Fig. 10. Plots of (a) log G' versus log ω and (b) log G'' versus log ω at 280 °C for: (○) neat PC, (△) 97.7/2.3 PC/Cloisite 30B nanocomposite, and (□) 95.7/4.3 PC/Cloisite 30B nanocomposite.

nanocomposites (compare Fig. 10a with Fig. 9a). In Fig. 10b, we also observe a pronounced effect of the concentration of Cloisite 30B on the G'' of PC/Cloisite 30B nanocomposites; namely, in the low frequency region (for $\omega <$ ca. 0.1 rad s^{-1}) values of G'' for the 95.7/4.3 PC/Cloisite 30B nanocomposite are about 1 order of magnitude greater than those for neat PC. Note that values of G'' for the 95.7/4.3 PC/Cloisite Na^+ nanocomposite are less than those for neat PC (see Fig. 9b). The increase of G' at low values of ω with increasing concentration of Cloisite 30B from 2.3 to 4.6 wt%, observed in Fig. 10a, is attributable to the increased surface areas due to an enhanced dispersion, via hydrogen bonding, of layered silicate aggregates. That is, when the layered silicate aggregates are more well dispersed due to the presence of hydrogen bonds between the carbonyl groups in PC and the hydroxyl groups in MT2EtOH, the surface area of layered silicate platelets is expected to increase markedly as the amount of Cloisite 30B in a nanocomposite is increased from 2.3 to 4.3 wt%. The readers are reminded that in Fig. 3c we showed evidence of the formation of hydrogen bonds in the 95.7/4.3 PC/Cloisite 30B nanocomposite.

Fig. 11 shows log$|\eta^*|$ versus log ω plots at 240, 260, and 280 °C for 95.7/4.3 PC/Cloisite Na^+ nanocomposite, and 95.7/4.3 PC/Cloisite 30B nanocomposite, in which values of complex viscosity $|\eta^*|$ were calculated using $|\eta^*| = [(G'/\omega)^2 + (G''/\omega)^2]^{1/2}$. The following observations are worth noting in Fig. 11. The log$|\eta^*|$ versus log ω plot of the 95.7/4.3 PC/Cloisite Na^+ nanocomposite exhibits very mild shear-thinning behavior in the low frequency region (for $\omega <$ ca. 1 rad s^{-1}) and then Newtonian behavior in the higher frequency region (for $\omega >$ ca.1 rad s^{-1}). It is well established that highly filled (say higher than 40 wt% filler) molten thermoplastic polymers exhibit strong shear-thinning behavior ('yield behavior') at low shear rates in steady shear flow or at low angular frequencies in oscillatory shear flow [39]. It is interesting to observe in Fig. 11 that the 95.7/4.3 PC/Cloisite Na^+ nanocomposite containing 4.3 wt% natural clay exhibits mild 'yield behavior' at $\omega <$ ca. 1 rad s^{-1}. We attribute this observation to particle–particle interactions of layered silicate aggregates. Whether or not yield behavior may be

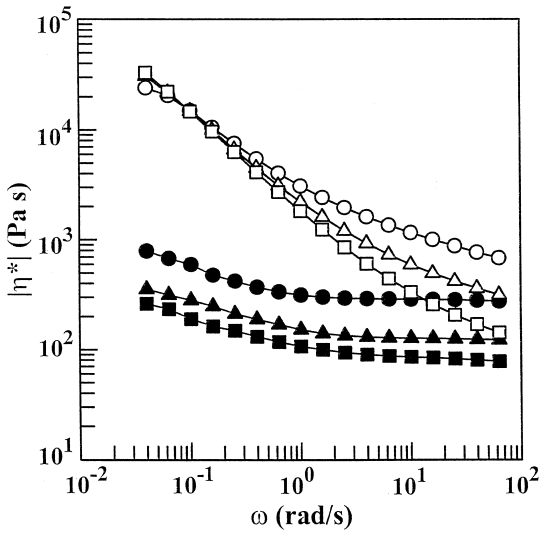

Fig. 11. Plots of log $|\eta^*|$ versus log ω for: (i) 95.7/4.3 PC/Cloisite Na^+ nanocomposite at 240 °C (●), 260 °C (▲), and 280 °C (■); (ii) 95.7/4.3 PC/Cloisite 30B nanocomposite at 240 °C (○), 260 °C (△), and 280 °C (□).

observed in a mixture of molten polymer and particulates would depend on the surface area of the particulates. The smaller the size of particulates (thus the larger the surface area of particulates) in a nanocomposite, the lower will be the concentration of the particulates that may give rise to yield behavior. Note that *little or no* specfic interactions exist between PC and the surface of natural montmorillonate in the 95.7/4.3 PC/Cloisite Na^+ nanocomposite.

The above argument must be modified when specfic interactions exist between the polymer matrix and the surface of layered silicates as in the PC/Cloisite 30B nanocomposites, where Cloisite 30B has hydroxyl groups that form hydrogen bonds with the carbonyl groups in PC. In Fig. 11 we observe very strong yield behavior in the 95.7/4.3 PC/Cloisite 30B nanocomposite over the entire range of ω and at all three temperatures, 240, 260, and 280 °C. Notice in Fig. 11 that the value of $|\eta^*|$ at $\omega = 0.03$ rad s^{-1} and at 280 °C for the 95.7/4.3 PC/Cloisite 30B nanocomposite is about 2 orders of magnitude greater than that for the 95.7/4.3 PC/Cloisite Na^+ nanocomposite. We attribute such a dramatic increase in $|\eta^*|$ to the presence of hydrogen bonds between the carbonyl groups in PC and the hydroxyl groups in MT2EtOH residing at the surface of the layered silicates of Cloisite 30B. The readers are reminded that in Fig. 3c we have shown evidence of the formation of hydrogen bonds in the 95.7/4.3 PC/Cloisite 30B nanocomposite.

Fig. 12 shows log G' versus log G'' plots for (a) 97.7/2.3 and 95.7/4.3 PC/Cloisite Na^+ nanocomposites at 240, 260, and 280 °C, and (b) 97.7/2.3 and 95.7/4.3 PC/Cloisite 30B nanocomposites at 240, 260, and 280 °C. It has amply been demonstrated that log G' versus log G'' plot is independent of temperature for homogeneous polymers [40,41] and also for heterogeneous polymer systems as long as the morphological state does not vary with temperature [42,43]. In this regard, log G' versus log G'' plot may be used

very effectively to determine whether or not the morphological state of a multiphase polymer system varies with temperature. Previously, Han and co-workers used log G' versus log G'' plot to determine order–disorder transition temperature of microphase-separated block copolymers [44–46] and clearing temperature of thermotropic liquid crystalline polymers [47,48]. Thus we can conclude from Fig. 12a that the morphological state of both 97.7/2.3 and 95.7/4.3 PC/Cloisite Na^+ nanocomposites changes little with temperature, because log G' versus log G'' plots of the nanocomposites have very weak temperature dependence. On the other hand, we can conclude from Fig. 12b that the morphological state of both 97.7/2.3 and 95.7/4.3 PC/Cloisite 30B nanocomposites varies with temperature, because log G' versus log G'' plots of the nanocomposites exhibit temperature dependence. Notice in Fig. 12b that log G' versus log G'' plot is shifted upward with increasing temperature and in the vicinity of $G'' = 100$ Pa values of G' at 280 °C for the 95.7/4.3 PC/Cloisite 30B nanocomposite are about 1 order of magnitude greater than those for the 97.7/2.3 PC/Cloisite 30B nanocomposites. This is not the case for the 97.7/2.3 and 95.7/4.3 PC/Cloisite Na^+ nanocomposites (see Fig. 12a). That is, the organoclay (Cloisite 30B) has a profound influence on the log G' versus log G'' plot (thus the morphological state) of the nanocomposites as a function of temperature, as compared to the natural clay (Cloisite Na^+).

The temperature dependence of log G' versus log G'' plots shown in Fig. 12 points out that time–temperature superposition (TTS) *fails* for the 97.7/2.3 and 95.7/4.3 PC/Cloisite 30B nanocomposites. Fig. 13 gives log G' versus log ω and log G'' versus log ω plots for 97.7/2.3 PC/Cloisite 30B nanocomposite at three different temperatures, 240, 260, and 280 °C, showing that the temperature dependence of log G' versus log ω plots is quite different from that of log G'' versus log ω plots (compare with Fig. 6 for PC). It is of great interest to observe in Fig. 13 that values of G' increase in the terminal region, while values of G'' decrease over the entire range of ω tested, as the temperature is increased from 240 to 280 °C. This is precisely the reason why log G' versus log G'' plots are shifted upward as the temperature is increased, as shown in Fig. 12b. No wonder why log G' versus log G'' plots (Fig. 12b) depend on temperature (i.e. why TTS fails) for the 97.7/2.3 PC/Cloisite 30B nanocomposite!

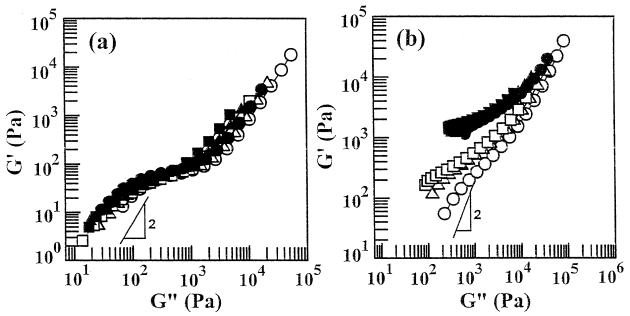

Fig. 12. Plots of log G' versus log G'' for: (a) 97.7/2.3 PC/Cloisite Na^+ nanocomposite at 240 °C (○), 260 °C (△), and 280 °C (□), and 95.7/4.3 PC/Cloisite Na^+ nanocomposite at 240 °C (●), 260 °C (▲), and 280 °C (■); (b) 97.7/2.3 PC/Cloisite 30B nanocomposite at 240 °C (○), 260 °C (△), and 280 °C (□), and 95.7/4.3 PC/Cloisite 30B nanocomposite at 240 °C (●), 260 °C (▲), and 280 °C (■).

Referring to Fig. 13, a question remains to be answered as to why the temperature dependence of log G' versus log ω plots is different from that of log G'' versus log ω plots for the PC/Cloisite 30B nanocomposites. The answer to this question lies in two factors: (i) the temperature dependence of compatibility between PC and Cloisite 30B, and (ii) the temperature dependence of the surface areas of the Cloisite 30B platelets. The fact that the log G' versus log G'' plots shown in Fig. 12b exhibit temperature dependence suggests that the PC/Cloisite 30B nanocomposites at 240, 260, and 280 °C must be regarded as being different materials from a rheological point of view.

Referring to Fig. 12b, the difference in log G' versus log G'' plots between the 97.7/2.3 and 95.7/4.3 PC/Cloisite 30B nanocomposites is attributable to the increased surface area as the amount of Cloisite 30B is increased from 2.3 to 4.3 wt%, which arose from the formation of hydrogen bonds between the carbonyl groups in PC and the hydroxyl groups in MT2EtOH. The readers are reminded that in Fig. 3c we presented evidence of the formation of hydrogen bonds in the 95.7/4.3 PC/Cloisite 30B nanocomposite, enhancing the compatibility between the PC matrix and the Cloisite 30B organoclay. We have learned that from the FTIR spectra shown in Fig. 3c it is very difficult to quantitatively determine the strength of hydrogen bonds and the population of hydrogen-bonded versus non-hydrogen-bonded carbonyls as the temperature is increased. The primary purpose of Fig. 3c is merely to show that hydrogen bonds between PC and Cloisite 30B persist over the entire range of test temperatures. Quantitative determination of the strength of hydrogen bonds and the population of hydrogen-bonded versus non-hydrogen-bonded carbonyls in the PC/Cloisite 30B nanocomposites are beyond the scope of this study. Thus, here we postulate that an increase in the surface areas of Cloisite 30B platelets with increasing temperature is responsible for the observed upward shift in log G' versus

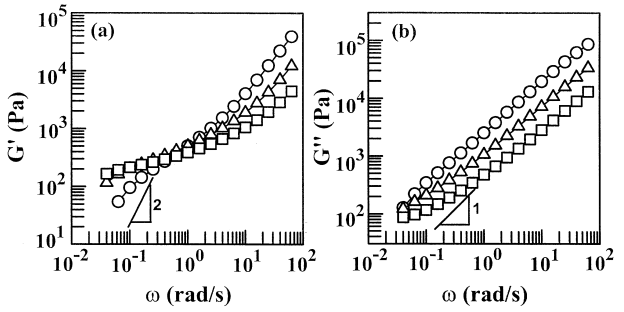

Fig. 13. Plots of (a) log G' versus log ω and (b) log G'' versus log ω for 97.7/2.3 PC/Cloisite 30B nanocomposite at various temperatures: (○) 240 °C; (△) 260 °C; (□) 280 °C.

log G'' plots with increasing temperature. An enhanced dispersion of Cloisite 30B aggregates with increasing temperature also came from a decrease in melt viscosity of PC in the nanocomposites as the temperature increased. It is estimated that the melt viscosity of PC decreased considerably (ca. 1 order of magnitude) as the temperature increased from 240 to 280 °C, which must have increased the mobility of PC molecules in the nanocomposites dramatically as the temperature increased from 240 to 280 °C. In turn, the markedly enhanced mobility of PC molecules must have helped to disperse Cloisite 30B aggregates in the nanocomposite as the temperature increased from 240 to 280 °C, giving rise to vastly increased surface areas of Cloisite 30B platelets. As a result, values of G' in the nanocomposite must have increased (in the low frequency region) as the temperature increased from 240 to 280 °C. The above observation explains why in Fig. 12b, values of G' of the 95.7/4.3 PC/Cloisite 30B nanocomposite are much greater than those of the 97.7/2.3 PC/Cloisite 30B nanocomposite.

The increase of G' in the 95.7/4.3 PC/Cloisite 30B nanocomposite, observed in Fig. 12b, cannot be ascribed to the formation of some kind of products from PC and any decomposition of gases formed from MT2EtOH at 240–280 °C, because referring to Fig. 8 we have already discussed the insignificant effect of thermal degradation of MT2EtOH on the oscillatory shear properties of PC/Cloisite 30B nanocomposites. If chain degradation of PC, for instance, had been extensive, we should have observed a decrease of G' in the PC/Cloisite 30B nanocomposite as the temperature was increased, because the smaller the size of macromolecules, the lower will be the values of G'. As a matter of fact, we conducted an isothermal TGA experiment at 280 °C for 1 h under a nitrogen atmosphere in order to find out the extent of thermal degradation of the 95.7/4.3 PC/Cloisite 30B nanocomposite. We found a weight loss of 0.6% after the isothermal TGA at 280 °C for 1 h, which cannot possibly explain the upward shift in the log G' versus log G'' plots shown in Fig. 12b. The weight loss, if were significant, should have brought the log G' versus log G'' plots downward, but not upward.

The only other possibility that can increase values of G' of the PC/Cloisite 30B nanocomposite with increasing temperature is crosslinking reactions of PC molecules themselves or chemical reactions between PC and MT2EtOH or the gases from MT2EtOH degradation. One may then suspect that crosslinking reactions during rheological measurements might have caused an upward shift in log G' versus log G'' plots for the 97.7/2.3 and 95.7/4.3 PC/Cloisite 30B nanocomposites shown in Fig. 12b. The most probable source of crosslinking reactions, which we can think of, would come from the unsaturated double bonds in the tallow of surfactant MT2EtOH residing at the surface of Cloisite 30B. As pointed out above, since the amount of unsaturated double bonds in the aliphatic chains of the tallow is so small (estimated to be less than 0.2 wt% in the 97.7/2.3 PC/Cloisite 30B nanocomposite and less than 0.5 wt% in the 95.7/4.3 PC/Cloisite 30B nanocomposite), it is highly unlikely that any crosslinking reactions of the unsaturated double bonds in the aliphatic chains of the tallow, if they occurred, could have increased the values of G' of the 97.7/2.3 PC/Cloisite 30B nanocomposite three fold only in the low frequency region, while decreasing the values of G' in the high frequency region, as the temperature increased from 240 to 280 °C (see Fig. 13a). Our argument lies in that crosslinking reactions would form a *permanent* three-dimensional network that would not be destroyed as the angular frequency is increased during oscillatory shear flow experiments. Further, as can be seen from Fig. 13b, the values of G'' of the same 97.7/2.3 PC/Cloisite 30B nanocomposite decreased as the temperature increased from 240 to 280 °C, which could not have happened if a significant degree of crosslinking reactions really occurred in the unsaturated double bonds of the tallow, ultimately shifting the log G' versus log G'' plots of 97.7/2.3 and 95.7/4.3 PC/Cloisite 30B nanocomposites upward as the temperature increased from 240 to 280 °C (see Fig. 12b).

3.7. Transient shear flow of PC/Cloisite Na^+ and PC/Cloisite 30B nanocomposites

In the present study, we probed rheological responses of PC/Cloisite Na^+ and PC/Cloisite 30B nanocomposites to transient shear flow. The transient shear flow experiment was motivated by the previous study of Mather et al. [49], who have shown that transient shear flow is very effective to probe evolution of the morphology of thermotropic liquid-crystalline polymers (TLCPs). Fig. 14 shows variations of shear stress growth ($\sigma^+(\dot{\gamma}, t)$) as a function of shear strain ($\dot{\gamma}t$), upon start-up of shear flow at 260 °C and $\dot{\gamma} = 1.0\ s^{-1}$, for (a) 95.7/4.3 PC/Cloisite Na^+ nanocomposite and (b) 95.7/4.3 PC/Cloisite 30B nanocomposite, where three separate runs, each using a fresh specimen denoted by different symbols, were made. Thus the three curves with different symbols shown in Fig. 14 represent variability of $\sigma^+(\dot{\gamma}, t)$ on three repeated measurements, showing successful application of strain scaling to nanocomposite transient shear data. Previously, Solomon et al. [25] reported on successful strain scaling to transient shear data for polypropylene/organoclay nanocomposites. According to Larson [50], the idea behind the use of strain scaling is that a microstructural relaxation time τ is manipulated by the applied strain with a form $\tau \sim \dot{\gamma}^{-1}$, where $\dot{\gamma}$ is the shear rate. In blends, this is due to droplet refinement and in liquid crystalline polymers this is due to disclination texture refinement. Thus, scaling shearing time by relaxation time suggests superposition of data at varying shear rates as t/τ or $\dot{\gamma}t$.

The following observations are worth noting in Fig. 14. Upon start-up of shear flow, both 95.7/4.3 PC/Cloisite Na^+ and 95.7/4.3 PC/Cloisite 30B nanocomposites exhibit an overshoot followed by monotonous decay reaching steady

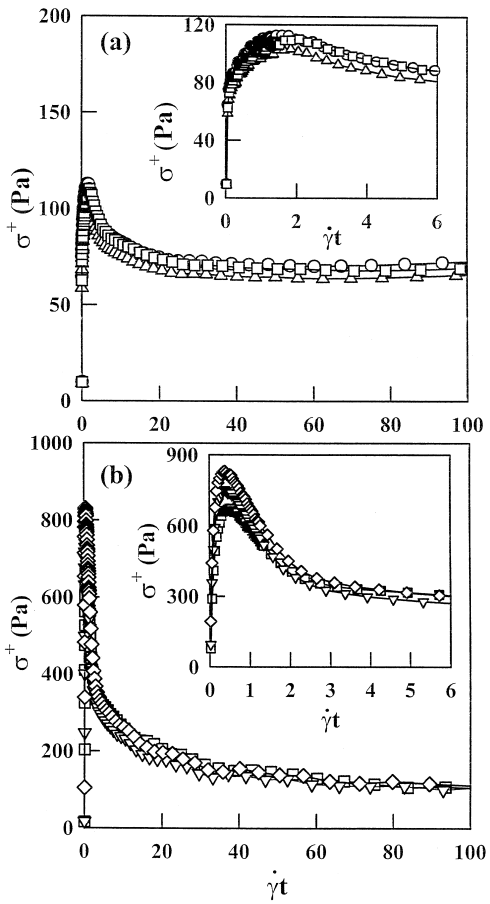

Fig. 14. Variations of $\sigma^+(\dot{\gamma},t)$ with $\dot{\gamma}t$ at 260 °C during transient shear flow at $\dot{\gamma}=1.0\ s^{-1}$ for: (a) 95.7/4.3 PC/Cloisite Na^+ nanocomposite for three repeated runs: (○) Run #1, (△) Run #2, and (□) Run #3; (b) 95.7/4.3 PC/Cloisite 30B nanocomposite for three repeated runs: (○) Run #1, (△) Run #2, and (□) Run #3.

state, and the magnitude of overshoot peak (σ^+_{peak}) for the 95.7/4.3 PC/Cloisite 30B nanocomposite is several times greater than that for the 95.7/4.3 PC/Cloisite Na^+ nanocomposite. We speculate that large σ^+_{peak} observed in the 95.7/4.3 PC/Cloisite 30B nanocomposite is due to strong attractive interactions (i.e. due to the presence of hydrogen bonds) between PC and surfactant at the surfaces of Cloisite 30B platelets, and small σ^+_{peak} observed in the 95.7/4.3 PC/Cloisite Na^+ nanocomposite is due to particle–particle interactions in the nanocomposite. The readers are reminded that in Fig. 3c we have shown evidence of the formation of hydrogen bonds in the 95.7/4.3 PC/Cloisite 30B nanocomposite.

Referring to Fig. 14, variability of σ^+_{peak} on three repeated runs is much greater in 95.7/4.3 PC/Cloisite 30B nanocomposite than in 95.7/4.3 PC/Cloisite Na^+ nanocomposite. This observation seems to suggest that a greater variability of the state of dispersion of Cloisite 30B aggregates exists in PC/Cloisite 30B nanocomposite than in PC/Cloisite Na^+ nanocomposite. Steady-state value of shear stress (σ) for the 95.7/4.3 PC/Cloisite 30B nanocomposite is about 60% greater than that for the 95.7/4.3 PC/Cloisite Na^+ nanocomposite. The above observations clearly indicate that Cloisite 30B has a much greater influence on the transient shear response of nanocomposite than natural clay, Cloisite Na^+. Variations of normalized shear stress growth ($\sigma^+(\dot{\gamma},t)/\sigma$) as a function of $\dot{\gamma}t$ (data not presented here) describe essentially the same characteristics as those described above in Fig. 14.

So far, we have not presented variations of first normal stress growth $N_1^+(\dot{\gamma},t)$ as a function of $\dot{\gamma}t$ for the nanocomposites investigated, although such information was provided in the previous study of Mather et al. for TLCPs [49]. The answer is very simple in that in steady-state shear flow the PC employed in the present study exhibited Newtonian behavior over the entire range of shear rates tested and thus has not exhibited measurable (and reproducible) values of first normal stress difference (N_1). The fact that the PC exhibits Newtonian behavior over the entire range of ω tested (0.04–100 rad s^{-1}) can be surmised from the log G'' versus log ω plots shown in Fig. 6b. Thus the addition of a natural montmorillonite or an organoclay (Cloisite 30B) to an inelastic Newtonian PC would not generate measurable (and reproducible) $N_1^+(\dot{\gamma},t)$ in transient shear flow. Indeed, in this study we have *not* observed reproducible $N_1^+(\dot{\gamma},t)$ signals during our transient shear flow experiments.

3.8. Intermittent shear flow of PC/Cloisite Na^+ and PC/Cloisite 30B nanocomposites

In the present study, we conducted intermittent shear flow experiments; namely a sudden shear flow was applied to a specimen after rest for a predetermined period upon cessation of steady shear flow. Such experiment has been found to be very useful to investigate the rheological response of TLCPs [51,52]. Fig. 15 shows variations of $\sigma^+(\dot{\gamma},t)$ as a function of $\dot{\gamma}t$ when a shear flow at $\dot{\gamma}=1.0\ s^{-1}$ was applied to (a) 95.7/4.3 PC/Cloisite Na^+ nanocomposite and (b) 95.7/4.3 PC/Cloisite 30B nanocomposite, after rest for different periods upon cessation of steady shear flow. It is seen in Fig. 15a that the evolution of $\sigma^+(\dot{\gamma},t)$ with $\dot{\gamma}t$ for 95.7/4.3 PC/Cloisite Na^+ nanocomposite is virtually independent of the duration of rest after cessation of steady shear flow. On the other hand, in Fig. 15b we observe that the duration of rest after cessation of steady shear flow has a profound influence on the evolution of $\sigma^+(\dot{\gamma},t)$ with $\dot{\gamma}t$ during intermittent shear flow of 95.7/4.3 PC/Cloisite 30B nanocomposite. Specifically, Fig. 15b shows that the value of σ^+_{peak} during intermittent shear flow of the 95.7/4.3 PC/Cloisite 30B nanocomposite increases with the duration of rest up to ca. 60 min and then levels off. This transient shear response is quite different from that observed in Fig. 15a for the 95.7/4.3 PC/Cloisite Na^+ nanocomposite. The above observations suggest that during rest up to about 60 min after cessation of steady shear flow, in the 95.7/4.3 PC/Cloisite 30B nanocomposite specific interactions persist,

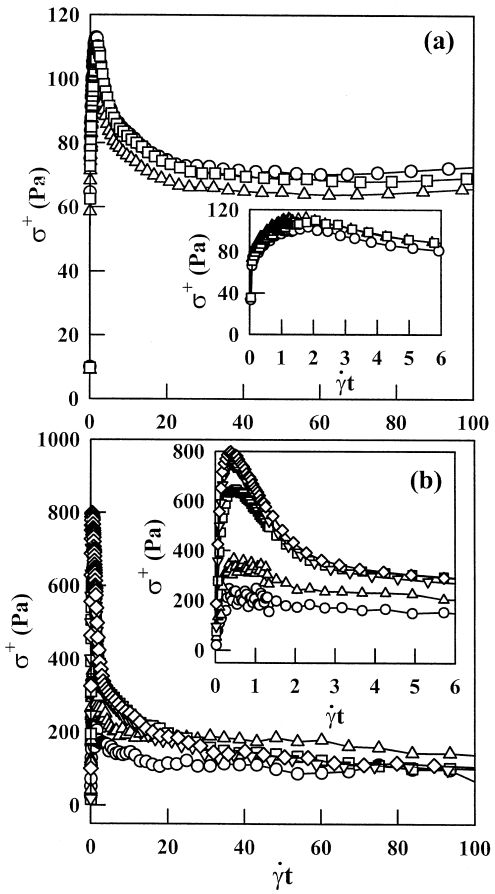

Fig. 15. Variations of $\sigma^+(\dot{\gamma}, t)$ with $\dot{\gamma}t$ at 260 °C during intermittent shear flow at $\dot{\gamma} = 1.0\ s^{-1}$ for: (a) 95.7/4.3 PC/Cloisite Na^+ nanocomposite after rest for different periods: (○) 5 min, (△) 30 min, and (□) 60 min; (b) 95.7/4.3 PC/Cloisite 30B nanocomposite after rest for different periods: (○) 5 min, (△) 15 min, and (□) 30 min, (▽) 60 min, and (◇) 90 min.

under quiescent conditions, between the hydroxyl groups in MT2EtOH of Cloisite 30B and the carbonyl groups in PC.

3.9. Steady-state shear viscosity of PC/Cloisite Na^+ and PC/Cloisite 30B nanocomposites

In the present study, we measured steady-state shear viscosity (η) of 95.7/4.3 PC/Cloisite Na^+ and 95.7/4.3 PC/Cloisite 30B nanocomposites, and the results are shown in Fig. 16. The accumulated strain in obtaining the steady-state shear viscosity shown in Fig. 16 is 600. In Fig. 16 we observe that 95.7/4.3 PC/Cloisite Na^+ nanocomposite exhibits weak shear-thinning behavior at $\dot{\gamma} < 1\ s^{-1}$ followed by Newtonian behavior at higher shear rates, while 95.7/4.3 PC/Cloisite 30B nanocomposite exhibits very strong shear-thinning behavior over the entire range of shear rates investigated. The dependence of η on $\dot{\gamma}$ shown in Fig. 16 is very similar to the dependence of $|\eta^*|$ on ω shown in Fig. 11. The differences in shear-rate dependence of viscosity between the 95.7/4.3 PC/Cloisite Na^+ and 95.7/4.3 PC/Cloisite 30B nanocomposites, observed in Fig. 16, can be explained by the same argument that was used to explain the differences in frequency dependence of complex viscosity between the two nanocomposites shown in Fig. 11.

3.10. Tensile properties of PC/Cloisite 30B and PC/Cloisite Na^+ nanocomposites

In this study we measured tensile properties of the 95.7/4.3 PC/Cloisite 30B and the 95.7/4.3 PC/Cloisite Na^+ nanocomposites, and the results are summarized in Table 1. It is seen in Table 1 that Young's modulus of the 95.7/4.3 PC/Cloisite 30B nanocomposite is 50% higher than that of the 95.7/4.3 PC/Cloisite Na^+ nanocomposite, and yield stress of the 95.7/4.3 PC/Cloisite 30B nanocomposite is 40% higher than that of the 95.7/4.3 PC/Cloisite Na^+ nanocomposite. The improved tensile properties of the 95.7/4.3 PC/Cloisite 30B nanocomposite is attributable to the presence of hydrogen bonds between the carbonyl groups in PC and the hydroxyl groups in MT2EtOH residing at the surface of silicate layers of organoclay Cloisite 30B.

4. Concluding remarks

When preparing clay-based nanocomposites by melt blending a thermoplastic polymer with layered silicates, two types of nanocomposites may be obtained: intercalated nanocomposite in which an extended polymer chain is intercalated between the host layers resulting in a well ordered multilayers, and exfoliated nanocomposite in which the layered silicates (ca. 1 nm thick) are exfoliated and dispersed in a continuous polymer matrix. Practically speaking, exfoliation is very difficult, if not impossible, owing to very high viscosity of molten thermoplastics. At best, one can expect to achieve reasonably well-dispersed

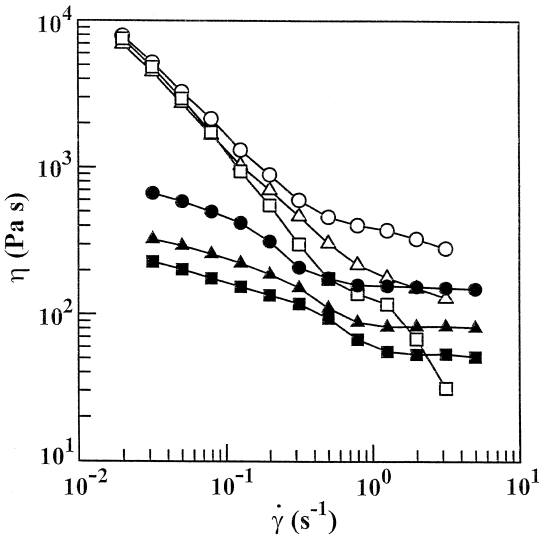

Fig. 16. Plots of log η versus log $\dot{\gamma}$ for: (i) 95.7/4.3 PC/Cloisite Na^+ nanocomposite at 240 °C (●), 260 °C (▲), and 280 °C (■); (ii) 95.7/4.3 PC/Cloisite 30B nanocomposite at 240 °C (○) ,260 °C (△), and 280 °C (□).

Table 1
Tensile properties of PC/Cloisite 30B and PC/Cloisite Na^+ nanocomposites

Sample code	Young's modulus (GPa)	Yield stress (MPa)	Elongation (%)
PC	1.2	39.9	16
95.7/4.3 PC/Cloisite Na^+	1.4	39.4	5
95.7/4.3 PC/Cloisite 30B	2.1	55.7	4

layered silicate of aggregates, the degree of dispersion being dependent upon the type of attractive interactions between layered silicate and polymer matrix. In the preparation of organoclays, layered silicates having a large active surface area ($700-800\ m^2\ g^{-1}$) and a moderate negative surface charge (cation exchange capacity) are treated chemically by replacing the hydrated metal cation in the pristine layered silicates with organic cations such as an alkylammonium and polar hydroxyl groups, and thus the layered silicates attain a hydrophobic/organophilic character. Because the negative charge originates in the layered silicates, the cationic head groups of the alkylammonium chloride molecule preferentially reside at the layer surface and the aliphatic tail will radiate away from the surface.

In this study, we investigated the rheology of PC/organoclay (Cloisite 30B) and PC/natural montmorillonite (Cloisite Na^+) nanocomposites. Cloisite 30B has hydroxyl groups at the end of the aliphatic tail (bis-2-hydroxyethyl). Thus, when Cloisite 30B was mixed with PC having carbonyl groups, the carbonyl groups formed hydrogen bonds with the hydroxyl groups of the aliphatic tail in the surfactant MT2EtOH, radiating from the layer surface and thereby enhancing compatibility between PC and Cloisite 30B platelets. One mechanism supporting the experimental results presented in this study is one where during melt blending the PC molecules penetrate between the layered silicate platelets, due to an enhanced compatibility, to better disperse the Cloisite 30B aggregates, and thus increase the surface area available for further attractive interactions. An alternative mechanism might be one of sequential peeling away of the top and bottom layers as promoted by polymer adsorption and the application of shear stress. Regardless of which of the two mechanisms postulated above is more reasonable than the other, what is clear here is that the inherent incompatibility between the pristine layered silicates and PC molecules was *modified* when PC was mixed with Cloisite 30B, because the PC molecules with carbonyl groups formed hydrogen bonds with the hydroxyl groups in MT2EtOH residing at the surface of Cloisite 30B. This is precisely the reason why in the present study dramatic differences in the linear dynamic viscoelastic properties and non-linear rheological properties were observed between the PC/Cloisite 30B and PC/Cloisite Na^+ nanocomposites. Thus we conclude that rheology is a very useful tool to probe the effectiveness of compatibilization between the aggregates of layered silicates and polymer matrix during melt blending.

Specifically, an increase in dynamic moduli (G' and G'' at low ω) with increasing concentrations of organoclay Cloisite 30B was observed in the 95.7/4.3 PC/Cloisite 30B nanocomposite (see Fig. 10). We attribute this to an increase in the surface area of dispersed layered silicates of Cloisite 30B platelets as the concentration of Cloisite 30B is increased. Consequently, as the number of sites available for hydrogen bonding between the carbonyl groups in PC and the hydroxyl groups in MT2EtOH of Cloisite 30B increases, values of G' and G'' in the nanocomposites are expected to increase. In the 95.7/4.3 PC/Cloisite 30B nanocomposite we have observed very high $|\eta^*|$ at very low ω in oscillatory shear flow (see Fig. 11) and very high η at very low $\dot{\gamma}$ in steady shear flow (see Fig. 16). We attribute this to the presence of hydrogen bonds between the carbonyl groups in PC and the hydroxyl groups in MT2EtOH of Cloisite 30B in the nanocomposites. In the 95.7/4.3 PC/Cloisite 30B nanocomposite we have observed a very large σ^+_{peak} upon start-up of shear flow. Again, we attribute this to the presence of hydrogen bonds between the carbonyl groups in PC and the hydroxyl groups in MT2EtOH of Cloisite 30B in the 95.7/4.3 PC/Cloisite 30B nanocomposites. In intermittent shear flow of 95.7/4.3 PC/Cloisite 30B nanocomposite, we observed a large increase in σ^+_{peak} with the period of rest after cessation of shear flow, indicating that structure evolution in the 95.7/4.3 PC/Cloisite 30B nanocomposite took place under quiescent conditions upon cessation of shear flow. This observation indicates further that hydrogen bonds between the carbonyl groups in PC and the hydroxyl groups in MT2EtOH of Cloisite 30B reformed, during rest upon cessation of shear flow, in the 95.7/4.3 PC/Cloisite 30B nanocomposites.

Of particular interest in the present study is an upward shift observed in the $\log G'$ versus $\log G''$ plots of PC/Cloisite 30B nanocomposites, while the $\log G'$ versus $\log G''$ plots of PC/ Cloisite Na^+ nanocomposites remain virtually unchanged, as the temperature is increased from 240 to 280 °C. We have attributed the observed upward shift in the $\log G'$ versus $\log G''$ plots of PC/Cloisite 30B nanocomposites to an increase in the surface areas of organoclay platelets due to an enhanced compatibility (via hydrogen bonding) between the matrix PC and the organoclay Cloisite 30B. We have ruled out the possibility that any crosslinking reactions of the unsaturated double bonds in the aliphatic chains of the tallow in the surfactant MT2EtOH, residing at the surface of the organoclay Cloisite 30B, could have caused the observed shift in the $\log G'$ versus $\log G''$ plots of PC/Cloisite 30B nanocomposites. The reason is that the amount of unsaturated double bonds in the aliphatic chains of the tallow is estimated to be extremely small; less than 0.2 wt% in the 97.7/2.3 PC/Cloisite 30 nanocomposite and less than 0.5 wt% in the 97.7/2.3 PC/Cloisite 30B nanocomposite. We do *not* wish to give the readers the impression that an upward shift in the $\log G'$ versus $\log G''$ plots of organoclay nanocomposites with increasing temperatures, observed in Fig. 12b for PC/

Cloisite 30B nanocomposites, will be observed only in the situations where hydrogen bonding taking place between a polymer matrix and an organoclay. Such temperature dependence of $\log G'$ versus $\log G''$ plots can also be observed in organoclay nanocomposites, where no hydrogen bonding takes place between the matrix phase and an organoclay. In other words, an upward shift in the $\log G'$ versus $\log G''$ plots of organoclay nanocomposites with increasing temperatures can be observed when the surface areas of organoclay platelets in the nanocomposite are increased with increasing temperatures. In a future publication we will report on such experimental observations.

It must be emphasized that a better understanding of the underlying microstructure of Cloisite 30B is necessary in order to develop commercially viable organoclay nanocomposites with thermoplastic polymers other than polycarbonate employed in the present study. The highlights of the rheological investigation conducted in this study can be summarized as follows. (i) The morphology of organoclay nanocomposites may be temperature dependent as determined from the temperature dependence of $\log G'$ versus $\log G''$ plots. (ii) Organoclay platelets exfoliate to a degree that is temperature dependent (mediated by polymer adsorption) and capable of mechanical percolation as in a house of cards. (iii) Strain scaling is obeyed for the organoclay nanocomposites investigated in this study. In this study, we interpreted our rheological results on the basis of molecular length scale (hydrogen bonding), but other interpretations can be made on the basis of larger length scale considerations (such as platelet bridging by chains or platelet network percolation). The amount of experimental results summarized in this paper may not be sufficient for one to make a generalization of the rheology of organoclay nanocomposites. Additional experimental study is needed in the future, which hopefully will stimulate fundamental theoretical study of layered silicate nanocomposites.

There are a number of organoclays available commercially. The choice of an organoclay must be made in such a way, that compatibility may be induced between an organoclay and polymer matrix. In this paper we have shown that during melt blending of PC with Cloisite 30B, compatibilization was accomplished through hydrogen bonding between the carbonyl groups in PC and the hydroxyl groups in the surfactant MT2EtOH present at the surface of Cloisite 30B.

Before closing, we wish to mention that functional group(s) in a polymer is not always necessary to prepare exfoliated or well-dispersed nanocomposites, as long as *attractive* interaction between the polymer and layered silicates can be induced. Ionic interactions between a polymer and layered silicates can be considered as such an example. One should explore other mechanisms that would induce attractive interactions between a polymer and layered silicates to achieve exfoliation in the preparation of nanocomposites.

Acknowledgements

We wish to acknowledge with gratitude very detailed and valuable comments by two anonymous reviewers, which helped us very much to improve the original manuscript. We also wish to acknowledge that Southern Clay Products provided us with the montmorillonite and organoclay employed in this study. This study was supported in part by LG Chemical Ltd.

References

[1] Usuki A, Kawasumi M, Kojima Y, Fukushima Y, Okada A, Kurauchi T, Kamigaito O. J Mater Res 1993;8:1174.
[2] Yano K, Usuki A, Okada A, Kurauchi T, Kamigaito O. J Polym Sci, Polym Chem Ed 1993;31:2493.
[3] Kojima Y, Usuki A, Kawasumi M, Okada A, Kurauchi T, Kamigaito O. J Polym Sci, Polym Chem Ed 1993;31:983.
[4] Kojima Y, Usuki A, Kawasumi M, Okada A, Kurauchi T, Kamigaito O, Kaji K. J Polym Sci, Polym Phys Ed 1994;32:625.
[5] Kojima Y, Usuki A, Kawasumi M, Okada A, Kurauchi T, Kamigaito O, Kaji K. J Polym Sci, Polym Phys Ed 1995;33:1039.
[6] Reynaud E, Jouen T, Gauthier C, Vigier G, Varlet J. Polymer 2001;42:8759.
[7] Sikka M, Cerini LN, Ghosh SS, Winey KI. J Polym Sci, Polym Phys Ed 1996;34:1443.
[8] Hasegawa N, Okamoto H, Kawasumi M, Usuki A. J Appl Polym Sci 1999;74:3359.
[9] Kato M, Usuki A, Okada A. J Appl Polym Sci 1997;66:1781.
[10] Kawasumi M, Hasegawa N, Kato M, Usuki A, Okada A. Macromolecules 1997;30:6333.
[11] Hasegawa N, Kawasumi M, Kato M, Usuki A, Okada A. J Appl Polym Sci 1998;67:87.
[12] Liu X, Wu Q. Polymer 2001;42:10013.
[13] Nam PH, Maiti P, Okamoto M, Kotaka T, Hasegawa N, Usuki A. Polymer 2001;42:9633.
[14] Ogata N, Jimenez G, Kawai H, Ogihara T. J Polym Sci, Polym Phys Ed 1997;35:389.
[15] Ogata N, Kawakage S, Ohihara T. Polymer 1997;38:5115.
[16] Liu YJ, Schindler JL, DeGroot DC, Kannewurf CR, Hirpo W, Kanatzidis MG. Chem Mater 1996;8:525.
[17] Sur GS, Sun HL, Lyu SG, Mark JE. Polymer 2001;42:9783.
[18] Vaia RA, Giannelis EP. Macromolecules 1997;30:7990.
[19] Vaia RA, Giannelis EP. Macromolecules 1997;30:8000.
[20] Lyatskaya Y, Balazs AC. Macromolecules 1998;31:6676.
[21] Balazs AC, Singh C, Zhulina E. Macromolecules 1998;31:8370.
[22] Balazs AC, Singh C, Zhulina E, Lyatskaya Y. Acc Chem Res 1999;32:651.
[23] Kuznetsov VD, Balazs CA. J Chem Phys 2000;112:4365.
[24] Lim YT, Park OO. Rheol Acta 2001;40:220.
[25] Solomon MJ, Almusallam AS, Seefeldt KF, Somwangthanaroj A, Varadan P. Macromolecules 2001;34:1864.
[26] Galgali G, Ramesh C, Lele A. Macromolecules 2001;34:852.
[27] Krishnamoorti R, Giannelis EP. Macromolecules 1997;30:4097.
[28] Giannelis EP, Krishnamoorti R, Manias E. Adv Polym Sci 1999;138:107.
[29] Krishnamoorti R, Giannelis EP. Langmuir 2001;17:1448.
[30] Hoffmann B, Kressler J, Stöppelmann G, Fredrich C, Kim GM. Colloid Polym Sci 2000;278:629.
[31] Lepoittevin B, Pantousher N, Devalckenaere M, Alexandre M, Kubies D, Calberg D, Jérôme K, Dubois P. Macromolecules 2002;35:8385.
[32] Physical Properties Bulletin from the Southern Clay Products, Inc.

[33] Coleman MM, Graf JF, Painter PC. Specific interactions and the miscibility of polymer blends. Lancaster: Technomic; 1991.
[34] Painter PC, Coleman MM. Fundamentals of polymer science, 2nd ed. Lancaster: Technomic; 1997. p. 172.
[35] Abbate M, Martuschelli E, Musto P, Ragosta G, Scarinzi G. J Polym Sci, Polym Phys Ed 1994;32:395.
[36] Lee KM, Han CD. Macromolecules 2003;36:804.
[37] Xie W, Gao Z, Pan WP, Hunter D, Singh A, Vaia RA. Chem Mater 2001;13:2979.
[38] Xie W, Gao Z, Pan WP, Lie K, Vaia RA, Hunter D, Singh A. Thermochim Acta 2001;367:339.
[39] Han CD. Multiphase flow in polymer processing. New York: Academic Press; 1981. Chapter 3.
[40] Han CD, Lem KW. Polym Engng Rev 1982;2:135.
[41] Han CD, Jhon MS. J Appl Polym Sci 1986;32:3809.
[42] Chuang K, Han CD. J Appl Polym Sci 1984;29:2205.
[43] Han CD. J Appl Polym Sci 1985;30:4431.
[44] Han CD, Kim J. J Polym Sci, Polym Phys Ed 1987;25:1741.
[45] Han CD, Kim J, Kim JK. Macromolecules 1989;22:383.
[46] Han CD, Baek DM, Kim JK. Macromolecules 1990;23:561.
[47] Kim SS, Han CD. Macromolecules 1993;26:3176.
[48] Kim SS, Han CD. Polymer 1994;35:93.
[49] Mather P, Jeon HG, Han CD, Chang S. Macromolecules 2000;33:7579.
[50] Larson RG. The structure and rheology of complex fluids. New York: Oxford University Press; 1977.
[51] Han CD, Kim SS. J Rheol 1994;38:13.
[52] Lee KM, Han CD. Macromolecules 2002;35:6263.